Microstructure Observation of Oxidation of Nd-Magnet at High Temperatures

Muhamad Firdaus, M. Akbar Rhamdhani, Yvonne Durandet, W. John Rankin, Kathie Mcgregor and Nathan A.S. Webster

Abstract There is a growing interest in recycling/recovery of rare earth elements from permanent magnets. A number of processing techniques are currently being developed but highly sensitive to the oxidation state of rare earth in the magnetic waste. This study investigated the microstructural changes of thermal oxidation of an Nd-based magnet and the behaviour of its oxides under high temperature recycling/recovery process. XRD analyses were carried out on a powdered sample ($\sim$10 μm) heated to 1273 K. SEM-EDS analysis was conducted on the heated bulk samples to provide detailed metallographic information. Metallographic analysis revealed multiple oxidation zones where the outer scale did not effectively inhibit further diffusion of oxygen. The thickness of this scale was found to be grown quite rapidly at temperatures higher than 973 K. The results indicated that the micro-mechanism of oxidation at higher temperature are more complex than at temperature below 773 K.

Keywords NdFeB magnet · Microstructure · Oxidation

Introduction

A number of processing techniques and strategies are currently being developed to recycle or recover the rare earth elements (REE) such as Nd, Dy and Pr from rare earth permanent magnets (REPM). Different processing routes such as hydrometallurgical, pyrometallurgical, physical/mechanical separation can be applied depending on the stage at which the recycled or end of life (EoL) products come into the material flow [1, 2]. All of these processing routes require significant

M. Firdaus (✉) · M. Akbar Rhamdhani · Y. Durandet
Department of Mechanical and Product Design, Swinburne University of Technology, Melbourne, VIC 3122, Australia
e-mail: mfirdaus@swin.edu.au

M. Firdaus · W. John Rankin · K. Mcgregor · N.A.S. Webster
CSIRO Mineral Resources, Private Bag 10, Clayton South, VIC 3169, Australia

© The Minerals, Metals & Materials Society 2017

H. Kim et al. (eds.), *Rare Metal Technology 2017*,
The Minerals, Metals & Materials Series,
DOI 10.1007/978-3-319-51085-9_7

understanding of the oxidation process of REPM at high temperature including its melting state in order for processes to be viable. There is currently a lack of information on the formation mechanisms and behaviour of the rare earth oxides in the waste REPM at high temperature. Oxidation observations were often done to support kinetics of reaction for specific techniques (e.g. in hydrometallurgy for leaching kinetics) without any attempt to understand the mechanisms. In addition, most investigations relied on the information from low temperature systems.

The corrosion and oxidation behaviour of REPM have been extensively studied particularly the degradation of magnetic properties at temperatures up to 873 K. The first report by Blank and Adler showed that oxidation between 673 and 873 K resulted in the formation of a grey layer on the surface of the bulk magnets and that its thickness increased parabolically with oxidation time [3]. The result showed that rapid surface oxidation with formation of a thin powdered layer on uncoated REPM takes place within the first minute and this can be substantial as the average particle size decreases [4–6]. This surface oxide layer does not effectively inhibit further diffusion of oxygen. Later work on the oxide microstructure of bulk NdFeB magnets was carried out by Breton and Edgley et al. [7, 8] mainly using SEM, XRD, and conversion electron mössbauer spectroscopy (CEMS) to identify the oxidation products. It was indicated in the report that the main reaction was the dissociation of the $Nd_2Fe_{14}B$ phase into α-Fe nanocrystals, Fe_2B and small Nd-oxide particles as follows:

$$2\mathrm{Nd(s)} + 3/2\mathrm{O_2(g)} \rightarrow \mathrm{Nd_2O_3(s)} \quad < 500\ \mathrm{K} \tag{1}$$

$$\mathrm{Nd_2Fe_{14}B(s)} + 3/2\mathrm{O_2} \rightarrow 14\mathrm{Fe(s)} + \mathrm{B(s)} + \mathrm{Nd_2O_3(s)} \quad < 500\ \mathrm{K} \tag{2}$$

$$2\mathrm{Fe(s)} + 3/2\mathrm{O_2(g)} \rightarrow \mathrm{Fe_2O_3(s)} \quad < 750\ \mathrm{K} \tag{3}$$

$$\mathrm{Fe_2O_3(s)} + \mathrm{Nd_2O_3(s)} \rightarrow 2\mathrm{FeNdO_3(s)} \quad > 750\ \mathrm{K} \tag{4}$$

Although the oxidation products were too fine, it was established later on using SEM and transmission electron microscopy (TEM) that the dominant grey zone formed on these alloys is, in fact, a zone of internal oxidation (IOZ) consisting principally of an α-Fe matrix containing Nd-oxide particles [3, 9–11]. Li et al. [3], Skulj et al. [12] and others [13–17] further studied the microstructures of the material to help understand the mechanism of oxidation. Based on their reports there was no degradation of the $Nd_2Fe_{14}B$ phase in the grains found using CEMS, and analysis by TEM confirmed that dissociation of the grain is unlikely and happens only when it reacts with oxygen [5].

The principal objective of this present study is to observe and evaluate the change in the microstructure of a commercial NdFeB alloy during oxidation in air at temperatures in the range 773–1273 K by using Scanning Electron Microscope (SEM) and X-ray diffraction (XRD). This will provide information that is useful for understanding the oxidation mechanism of waste NdFeB magnets at high

temperature, and in return to improve the strategy and techniques in recovering the REE or recycling the REPM.

Experimental Methodology

Materials

Sintered N45-NdFeB magnets used in the current study were supplied by Alpha Magnetics Ltd. and had a nominal composition within the range given in Table 1 with platted nickel for coating. The clean magnet was thermally demagnetised at 573 K in a Nabertherm TR 60 oven furnace and samples with dimension of $10 \times 5 \times 5$ mm were produced by cutting the magnets using a Struers Secotom-15/-50 high performance cut-off machine. The nickel coating was removed manually after cutting using abrasive papers. The bulk composition of the demagnetised magnet sample, derived from inductively coupled plasma (ICP-AES) analysis is shown in Table 1. The typical cross sectional microstructure of the initial sample is shown in Fig. 1a, b. The back-scattered electron (BSE) micrograph of the unreacted sample shown in Fig. 1b indicates the two major phases typical of a Nd–Fe–B magnet system; the ϕ phase ($Nd_2Fe_{14}B$) matrix, indicated by (A) and Nd-rich phase at the grain boundary, indicated by (B). A small amount of η phase ($Nd_1Fe_4B_4$) is also present (indicated by C) as can be seen in Fig. 1a.

Approach and Parameters

For the high temperature experiments the surfaces of the samples were ground using a 1200-grade SiC paper and cleaned ultrasonically in acetone prior to oxidation. The samples were placed in a 4-cm diameter alumina crucible and oxidation was carried out in an air atmosphere in a Nabertherm LT 15/13/P330 muffle furnace. Four crucibles were placed in the hot zone of the furnace after the temperature of the furnace reach the set point and different samples were taken out after different set of hours. The samples were cooled in ambient air and then placed inside 1 ml LLG shell vials before conducting metallographic analysis. It is reasonable to assume that further oxidation do not occur under ambient conditions (e.g. at room temperature) due to kinetic limitation.

Table 1 Chemical composition of REPM sample (mass%)

	Nd	Pr/Dy	Fe	B
Typical composition commercial magnet	23–31	0–7	65–70	0.9–1.2
Bulk composition of sample used in the study	22.4	8.5	68	1

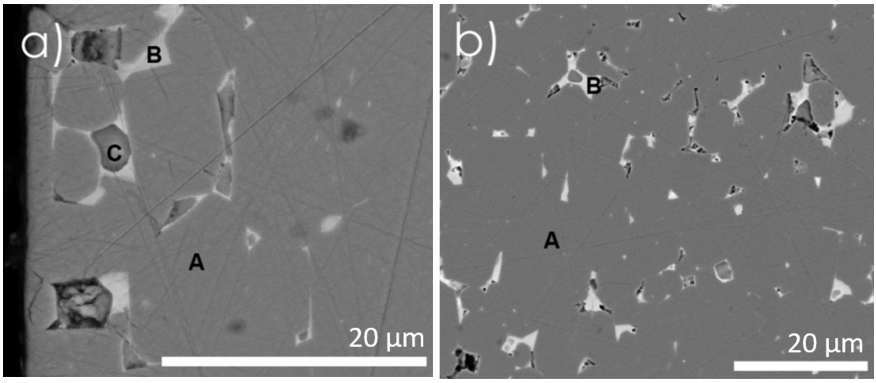

Fig. 1 Backscattered electron (BSE) images from the un-oxidised (Nd, Pr)2Fe14B starting material: **a** a region close to the sample surface, and **b** the central region of the sample. The dark region on **a** is the epoxy resin mounting medium

Post Experiment Sample Preparation

The samples pre and post-oxidation were analysed using different characterization techniques which included SEM, energy dispersive X-ray spectroscopy (EDX), XRD, and ICP. For the SEM and EDX analysis, a FEI Quanta 400F Environmental Scanning Electron Microscope (ESEM) was used. The samples preparation for the SEM analysis include mounting of the samples in an epoxy resin in 2.5-cm round blocks before being cured at 60 °C overnight, sectioned to expose a fresh surface, and then polished flat using successively finer diamond paste compounds down to a final polishing size of 1 µm. Immediately prior to analysis, each sample was coated with a ~5–10 nm thick carbon film to prevent charge build-up on the surface of the sample when probed by the electron beam. The SEM analysis was carried out using an accelerating voltage of 15 kV, a working distance of 10 mm, an emission current of 276 mA, and a vacuum of 2.8×10^{-6} Torr.

The samples were micronized in ethanol for 4 min g^{-1} and dried prior to XRD analysis. The XRD data were collected at 2θ angles from 5 to 140°, using a PANalytical MPD instrument fitted with a cobalt long-fine-focus X-ray tube operated at 40 kV and 40 mA. The incident beam path was defined using 0.04 rad Soller slits, a 20 mm mask, a 0.5° fixed divergence slit, and a 1° anti scatter slit. The diffracted beam incorporated a second set of Soller slits, a graphite monochromator to eliminate unwanted wavelengths and a 4.6 mm anti-scatter slit. An X'Celerator detector was used in scanning line (1D) mode with an active length of 2.122° 2θ. Approximate phase concentrations were calculated from the XRD data via the Rietveld method.

Results and Discussion

The XRD data for samples prior and after ~24 h oxidation at 973 and 1173 K are presented in Fig. 2. The approximate phase concentrations calculated from the XRD data using Rietveld method is presented in Table 2. The data for the unheated (un-oxidised) sample contain peaks indicative of $Nd_2Fe_{14}B$, as well as minor peaks (marked with * in Fig. 2) for which phase assignment could not be conclusively made. The XRD spectra for the 973 and 1173 K oxidised samples contain peaks for α-Fe, iron oxides and $NdFeO_3$, suggesting that the reaction from Eqs. (1) to (4) proceed and for the 1173 K sample also contains peaks indicative of $NdBO_3$. There was no evidence for the formation of pure Nd_2O_3 during oxidation but rather the formation of $FeNdO_3$ which suggests that Nd_2O_3 formed a solid solution with Fe_2O_3 in accordance with Eq. (4). However, the results show an increase of Fe_2O_3

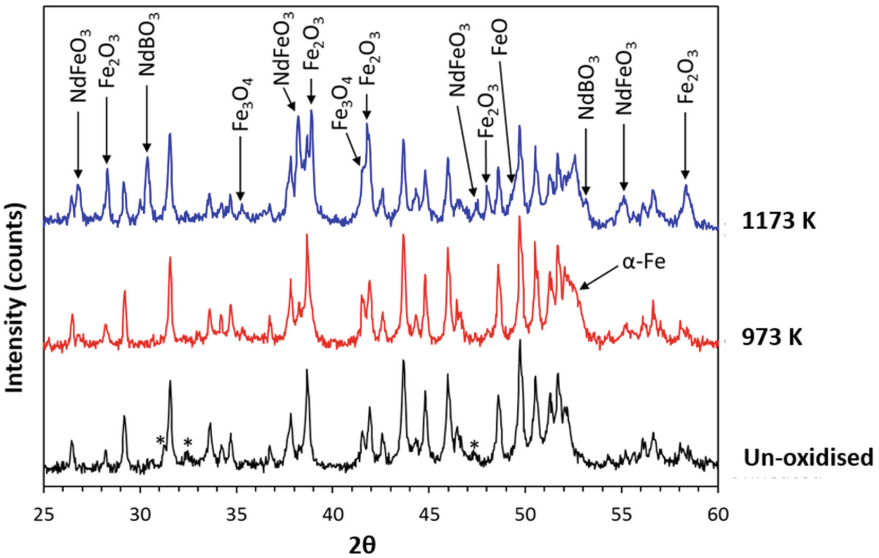

Fig. 2 XRD data collected for the unheated (un-oxidised) sample, and the samples oxidised at 973 and 1173 K. Datasets offset in the intensity axis for clarity. Significant peaks for the oxidisation phases are labelled in the 973 and 1173 K plots; in the un-oxidised plot all of the peaks are assigned to $Nd_2Fe_{14}B$ except the minor peaks annotated with *

Table 2 Summary of phase quantification results from the XRD data

Samples	Phase (wt%)						
	$Nd_2Fe_{14}B$	Fe_2O_3	Fe_3O_4	FeO	Fe	$NdFeO_3$	$NdBO_3$
Original	~100						
973 K	74	6	4		13	3	
1173 K	44	22	7	3	8	10	5

and Fe_3O_4 during oxidation, and the 1173 K sample also appeared to contain FeO that may indicate that the formation of $FeNdO_3$ (Eq. 4) may not be instantaneous or there were not enough Nd_2O_3 in the oxidised zone.

The typical morphology of the oxidation product at 773 K is shown in Fig. 3. The oxidation of Nd–Fe–B magnets at 773 K appeared to follow a typical gas–solid reaction. The oxidation reactions at this temperature resulted in the formation of an external scale (external oxidation zone—EOZ) and a grey dense internally oxidised zone (IOZ), which is an order of magnitude thicker than the surface oxide layers and represents the main form of degradation resulting from the oxidation reactions. The depth of external oxidation zone (EOZ) was found to be constant with increasing time and not effectively inhibit further diffusion as seen in Fig. 4. This observation is consistent with earlier investigations carried out by Li et al. [3], Skulj et al. [12] Edgley et al. [7, 8] and others [13–17].

The oxidation process at higher temperature above 973 K resulted in a more complex morphology as seen in Fig. 5, which shows a cross section of a sample oxidised for 60 h at 1173 K from its edge to the centre. On the surface of the sample, a darker layer can be seen. This dark surface layer or the EOZ was more

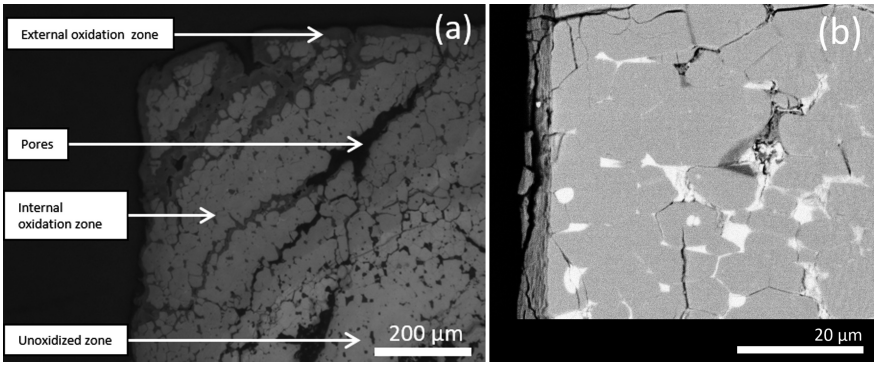

Fig. 3 Light microscope (**a**) and SEM backscattered electron image (**b**) showing typical cross-section microstructure of the oxidised layers of the NdFeB magnets heated at 773 K for 72 h

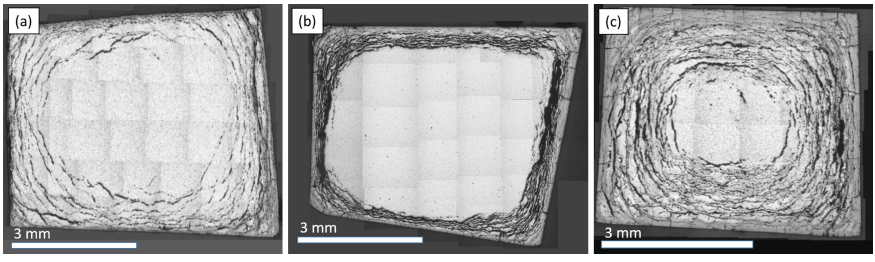

Fig. 4 Cross-section macrostructure showing the effect of oxidation time at 773 K, **a** t = 23 h, **b** t = 45 h, and **c** t = 72 h

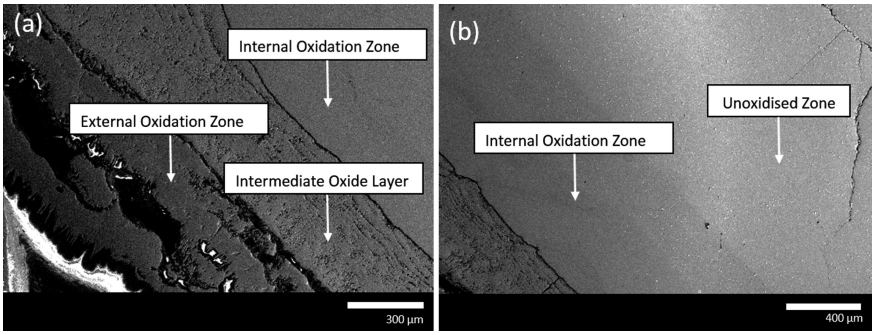

Fig. 5 Typical cross-section of the oxidised layers of the NdFeB magnets heated at 1173 K for 60 h showing **a** region close to the surface and **b** the central region of the sample

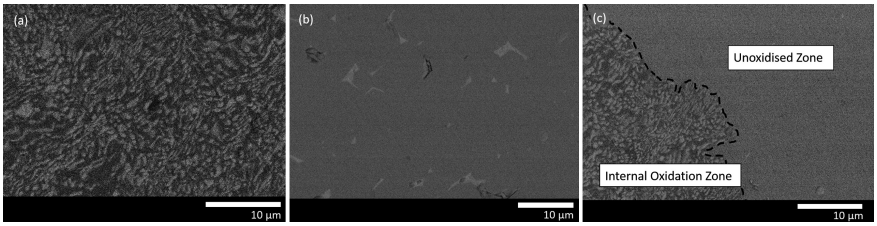

Fig. 6 SEM BSE images of microstructures of samples heated at 1173 K for 60 h **a** IOZ, **b** unreacted zone, and **c** transition between IOZ and unreacted zone (*dash line* for guide)

prominent compared to those observed at 773 K. This layer has grown outward considerably with time, unlike the EOZ observed in the oxidation at 773 K, and an expansion has taken place within this layer. Moving away from the edge the next layer is the second oxide layer (intermediate layer), which was not seen in the oxidation at 773 K, then followed by the grey IOZ. Unlike the microstructure at 773 K, the IOZ was completely different than the unreacted zone as seen in Fig. 6. The Nd-rich phase in the IOZ which was seen in the sample heated at 773 K (Fig. 3) appears to be reacted and dissolved into the IOZ in the sample heated at 1173 K. It should also be noted from the SEM topography that whilst the IOZ is fully dense, the EOZ and intermediate layer are porous with significant sign of presumably cracking due to density change upon cooling. An investigation using a high temperature microscope (result not shown here) supported the notion that this friability represents a mechanical damage induced during cooling.

Previous investigations at lower temperature indicate that there is no significant diffusion of Nd during oxidation [3, 4, 7, 8, 12]. Based on the investigation of the IOZ at temperature range of 600–773 K assuming that there is no access restriction of oxygen by the oxidised surface Li et al. [3] deduced that the permeability of oxygen in the oxidized zone is much larger than that of Nd. As such there will be minimum movement of Nd during the oxidation process unless microstructural

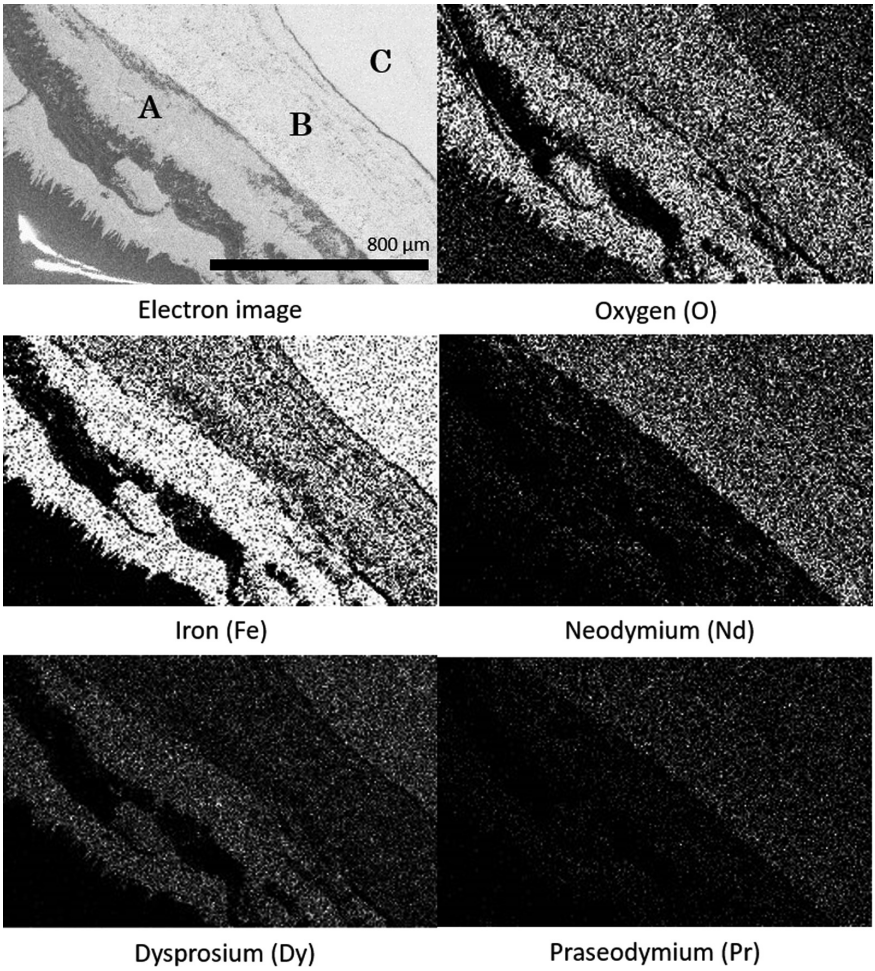

Fig. 7 EDS elemental mapping of the EOZ (**a**), intermediate layer (**b**) and IOZ (**c**) of sample heated at 1173 K, 60 h, brighter image represent high concentration

change occur. It is then expected that the effective Nd concentration remains essentially constant both within the oxidation zone and the un-oxidised substrate. This suggests that only oxygen or iron diffusing in or out of the core substance. It is believed that at temperature below 973 K the oxygen transport occurs by short-circuit diffusion and the most likely diffusion paths are the high-angle α-Fe grain boundaries. The α-Fe columnar grain structure coarsens as the oxidation front traverses an original alloy grain. This coarsening has been associated with the loss of relatively low-angle grain boundaries which carry less of the inward oxygen flux [12]. Furthermore, the previous studies on the oxidation at temperature below

973 K indicate that the ratio of iron to neodymium remains approximately constant, and that there is no evidence of outward diffusion of iron [3, 4, 7, 8, 12].

The EDS elemental mapping of the oxidation product layer depicted in Fig. 7 shows no neodymium in the outermost layer (EOZ) with considerably high concentration of iron and oxygen, suggesting that the layer consist of iron oxides (Fe_2O_3 or Fe_3O_4) as also indicated by the XRD result in Fig. 2. Figure 7 also shows that the intermediate layer (B) is an iron depleted region where the concentration of iron is lower compared to the EOZ (A) and IOZ (C). It is then evident with the growth of the EOZ then that there is outward diffusion of Fe from the intermediate layer to the EOZ. The oxygen concentration profiles across EOZ (A) and intermediate layer (B) are relatively constant with small reduction at the interface. The concentration reduces dramatically between the intermediate layer (B) interface and the IOZ (C). The interfaces are sharp and there is no gradual composition transition. Across the IOZ, moving further into the sample, there is a gradual reduction in oxygen concentration. It is also need to be noted that the distribution of Dy follows that of Fe whilst the distribution of Pr follows that of Nd.

Conclusions

Oxidations of NdFeB magnet have been carried out in an air atmosphere over the temperature range 773–1273 K. A different microstructural evolution was evident when comparing the samples oxidised at 773 and 1173 K. The microstructure of magnet oxidised at 773 K consists of dark outer layer (EOZ) and a grey internal oxidation zone that grow inwards with time. The oxidation process at higher temperature above 973 K resulted in a more complex microstructure with EOZ growing outwards and intermediate layer and IOZ growing inwards. Evidence of Fe depletion region shows that there is Fe diffusion to the outer scale (EOZ) which was not seen in the magnet oxidised at 773 K. The mechanism of oxidation may include both the diffusion of oxygen and iron into and out of the substrate, with further details on the matrix and diffusion path required. Further systematic study will need to be carried out to clarify the detailed oxidation mechanism of the NdFeB magnet.

Acknowledgements The authors are grateful to the CSIRO Minerals Resources for the financial support (top up scholarship for Mr Muhamad Firdaus) for this work. The authors would like to also thanks Dr. Mark Pownceby for the SEM analysis at CSIRO.

References

1. M. Firdaus et al., Review of high-temperature recovery of rare earth (Nd/Dy) from magnet waste, J. Sustain. Metall. (2016)
2. K. Binnemans et al., Recycling of rare earths: a critical review. J. Clean. Prod. **51**, 1–22 (2013)

3. Y. Li et al., The oxidation of NdFeB magnets. Oxid. Met. **59**(1–2), 167–182 (2003)
4. J. Jacobson, A. Kim, Oxidation behavior of Nd-Fe-B magnets. J. Appl. Phys. **61**(8), 3763–3765 (1987)
5. J.M. Le Breton, J. Teillet, Oxidation of (Nd, Dy)FeB permanent magnets investigated by 57Fe Mossbauer spectroscopy. IEEE Trans. Magn. **26**(5), 2652–2654 (1990)
6. E.D. Dickens, A.M. Mazany, The corrosion and oxidation of Nd-Fe-B magnets. J. Appl. Phys. **67**(9), 4613–4615 (1990)
7. D.S. Edgley et al., Dissociation of $Nd_2Fe_{14}B$ during high temperature oxidation. J. Magn. Magn. Mater. **128**, L1–L7 (1993)
8. D.S. Edgley et al., Characterisation of high temperature oxidation of $Nd_2Fe_{14}B$ magnets. J. Magn. Magn. Mater. **173**, 29–42 (1997)
9. K. Miura, M. Itoh, K.-I. Machida, Extraction and recovery characteristics of Fe element from Nd–Fe–B sintered magnet powder scrap by carbonylation. J. Alloy. Compd. **466**, 228–232 (2008)
10. T. Saito et al., The extraction of Nd from waste Nd–Fe–B alloys by the glass slag method. J. Alloy. Compd. **353**, 189–193 (2003)
11. M. Nakamoto et al., Extraction of rare earth elements as oxides from a neodymium magnetic sludge. Metall. Mater. Trans. B **43**(3), 468–476 (2012)
12. I. Skulj, H.E. Evans, I.R. Harris, Oxidation of NdFeB-type magnets modified with additions of Co, Dy, Zr and V. J. Mater. Sci. **43**(4), 1324–1333 (2008)
13. T.G. Woodcock et al., Understanding the microstructure and coercivity of high performance NdFeB-based magnets. Scripta Mater. **67**(6), 536–541 (2012)
14. H. Sepehri-Amin et al., Grain boundary and interface chemistry of an Nd–Fe–B-based sintered magnet. Acta Mater. **60**(3), 819–830 (2012)
15. L. Deshan et al., Grain boundary phase formation and magnetic properties of NdFeB/Nd multilayered films, Jpn. J. Appl. Phys. **48**(3) (2009)
16. E. Belin-Ferré, Basics of thermodynamics and phase transitions in complex intermetallics. Book Series on Complex Metallic Alloys. (World Scientific, Singapore, 2008)
17. W.Q. Liu et al., Oxidation kinetics of Nd-Fe-B permanent magnets prepared by spark plasma sintering. Corrosion **66**(5), 0550041–0550045 (2010)